Research in Astron. Astrophys. **2011** Vol. **11** No. **4**, 391–400
http://www.raa-journal.org *http://www.iop.org/journals/raa*

Research in Astronomy and Astrophysics

Multiwavelength Doppler factors for Fermi-detected gamma-ray loud blazars

Hou-Dun Zeng and Li Zhang

Department of Physics, Yunnan University, Kunming 650091, China; *houdunz@126.com*

Received 2010 September 30; accepted 2010 October 30

Abstract We collect a sample of 51 Fermi-detected gamma-ray loud blazars with known radio Doppler factors and study properties of the Doppler factors of blazars at optical, X-ray and gamma-ray bands. A basic assumption is that the emission from the radio to gamma-ray bands of the blazars are produced by the nonthermal radiation of accelerated particles in a jet. Our results show that (1) the Doppler factors of blazars are a function of frequency, with the Doppler factor decreasing with frequency from the radio to X-ray regions, and then increasing from the X-ray to γ-ray regions which are similar to results given by Zhang et al., and (2) there are marginal correlations between the Doppler factors at radio and X-ray bands and the synchrotron peak frequency, and a strong correlation between the Doppler factor in the gamma-ray band and the synchrotron peak frequency, but no correlation in the optical band.

Key words: galaxies: active — galaxies: nuclei — galaxies: jets — radiation mechanisms: non-thermal

1 INTRODUCTION

The Large Area Telescope (LAT) onboard the Fermi Gamma Ray Space Telescope (Fermi) has detected 709 active galactic nuclei (AGNs) (Abdo et al. 2010). These include 296 flat spectrum radio quasars (FSRQs), 300 BL Lac objects, 41 other types of AGNs, and 72 AGNs of unknown type. Observed spectral energy distributions (SEDs) of blazars (generally including FSRQs and BL Lac objects) indicate two main component features: the first one, peaking between the far infrared and the X-ray band, is generally believed to be produced by the synchrotron radiation of relativistic electrons in the jet; the second, peaking between 10 MeV – 100 GeV, is usually believed to be produced by Compton radiation from the same electrons producing the synchrotron component (e.g. Maraschi et al. 1992; Bloom & Marscher 1996; Sikora et al. 1994; Dermer et al. 1992; Ghisellini et al. 1998). There are many kinds of models for explaining nonthermal emission from gamma-ray loud blazars, for example, external Compton (EC) models (e.g. Dermer et al. 1992, 1997; Sikora et al. 1994; Zhang & Cheng 1997) and synchrotron self-Compton (SSC) models (e.g. Maraschi et al. 1992; Ghisellini 1993; Bloom & Marscher 1996).

All current models have been established in the frame of a jet of AGNs, i.e. the beaming models, therefore one of the important parameters is the Doppler factor of the jet, which is defined as $\delta = [\Gamma(1-(v/c)\cos\theta)]^{-1}$, where $\Gamma = [1-(v/c)^2]^{-1/2}$ is the bulk Lorentz factor, v is the jet speed, c is the speed of light, and θ is the angle between the jet and our line-of-sight. In the beaming models,

the relationship between the observed flux density $S_i^{\rm obs}$ in the ith band and the intrinsic flux density $S_i^{\rm int}$ is given by (e.g. Blandford & Königl 1979)

$$S_i^{\rm obs} = \delta_i^{\beta}(1+z)^{\alpha_i-1}S_i^{\rm int} \ , \tag{1}$$

where the factor $(1+z)^{\alpha_i-1}$ represents a K-correction, z is the redshift, α_i is the spectral index ($S_i \propto \nu_i^{\alpha_i}$), and β is a parameter depending on the shape of the emitted spectrum and the detailed physics of the jet (Lind & Blandford 1985); $\beta = 3+\alpha$ is for a moving sphere and $\beta = 2+\alpha$ is for the case of a continuous jet. It can be seen from Equation (1) that the Doppler factor is very important for estimating the intrinsic flux density of the source and then deriving the physical properties of the source. Although most of the previous beaming models assumed that the Doppler factor is a constant at all observed bands, the emissions from different regions may generally result in different possible Lorentz factors (Ghisellini & Maraschi 1989) and viewing angles (Ciliegi et al. 1995). Using a limited sample of gamma-ray loud blazars with known radio Doppler factors, Zhang et al. (2002) studied multiwavelength Doppler factors of blazars using a sample of 31 gamma-ray loud blazars and suggested that the Doppler factors are different at different wavebands. With improved observations in both radio and γ-ray bands, it is worth reconsidering this issue.

In this paper, we collect a sample of 51 gamma-ray loud blazars with known radio Doppler factors from the first Fermi catalog of AGNs given by Abdo et al. (2010). For the radio Doppler factors, we use the results estimated by Hovatta et al. (2009) and Savolainen et al. (2010). The radio Doppler factor can be expressed as (Savolainen et al. 2010)

$$\delta_{\rm R} = \delta_{\rm var} = \left[1.47\times10^{13}\frac{\Delta S_{\rm max} d_{\rm L}^2}{\nu^2\Delta t^2(1+z)T_{\rm b,int}}\right]^{1/3} \ , \tag{2}$$

where $\Delta S_{\rm max}$ is the flare amplitude in Janskys, ν is the observing frequency in GHz, Δt is the timescale of the fastest flare from the source in days, and $d_{\rm L}$ is the luminosity distance in Mpc. Using such a sample, we investigate the properties of the Doppler factor at different wavebands.

2 DATA COLLECTION AND SYNCHROTRON PEAK FREQUENCY

After comparing the first catalog of AGNs detected by the LAT (Abdo et al. 2010) with both the Metsahovi-MOJAVE sample (Savolainen et al. 2010) and a sample of AGNs from (Hovatta et al. 2009), we have collected a sample of 51 gamma-ray loud blazars with known radio Doppler factors. In this sample, the averaged radio flux densities are taken from Teräsranta et al. (2004); for the optical data and the X-ray data, some of them are taken from those complied by Fossati et al. (1998) and Cheng et al. (2000), and the others are obtained through the *VizieR Service*; redshifts, gramma-ray photon fluxes ($>$ 1GeV) and spectral indices of the blazars are taken from Abdo et al. (2010). For the gamma-ray data, we need to convert the gramma-ray photon flux into flux density at a given energy. Assuming $S(\nu_1,\nu_2)$ is the $\gamma-$ray energy flux between ν_1 and ν_2, it can be calculated from the photon flux $F_\gamma(E>1\,{\rm GeV})$ [ph cm^{-2} s^{-1}] as (Ghisellini et al. 1989, 1993, 1998)

$$S_\gamma(\nu_1,\nu_2) = \begin{cases} \frac{\alpha_\gamma h\nu_1 F_\gamma}{1-\alpha_\gamma}\left[(\frac{\nu_2}{\nu_1})^{1-\alpha_\gamma}-1\right] & \text{for } \alpha_\gamma \neq 1 \ , \\ h\nu_1 F_\gamma \ln(\nu_2/\nu_1) & \text{for } \alpha_\gamma = 1 \ . \end{cases} \tag{3}$$

Setting $\nu_1 = 2.42\times10^{23}$ Hz (1 GeV), $\nu_2 = 2.42\times10^{25}$ Hz (100 GeV), $F_\gamma = 10^{-8}F_{\gamma,-8}$ ph cm^{-2} s^{-1}, and $\alpha_\gamma = \Gamma_\gamma - 1$, Equation (3) can be rewritten as (in units of erg cm^{-2} s^{-1})

$$S_\gamma(1,100) = \begin{cases} 1.6\times10^{-11}\frac{\alpha_\gamma F_{\gamma,-8}}{1-\alpha_\gamma}\left(100^{1-\alpha_\gamma}-1\right) & \text{for } \alpha_\gamma \neq 1 \ , \\ 7.38\times10^{-11}F_{\gamma,-8} & \text{for } \alpha_\gamma = 1 \ . \end{cases} \tag{4}$$

Then the monochromatic flux at the average energy $\langle E\rangle$ is calculated by

$$S_\gamma(\langle E\rangle) = 10^{35}\frac{S_\gamma(1,100)(-\Gamma_\gamma+2)}{\nu_2^{-\Gamma_\gamma+2}-\nu_1^{-\Gamma_\gamma+2}}(\langle E\rangle\nu_1)^{-\Gamma_\gamma+1}\ \mathrm{pJy}\ . \tag{5}$$

In deriving the above equation, it is assumed that the γ-ray energy range is from 1 GeV to 100 GeV and that the average energy $\langle E\rangle$ of each object is in units of 1 GeV.

In Table 1, we give a list of 51 blazars, including 33 FSRQs and 18 BL Lac objects. In order to estimate the Doppler factor for each object, we require the peak frequency, $\nu_{\rm p}$, of synchrotron radiation in the SED of a blazar. Following Abdo et al. (2010), $\nu_{\rm p}$ for each object can be estimated in the $\alpha_{ox}-\alpha_{ro}$ plane (see also Padovani & Giommi 1995; Padovani et al. 2003), which is

$$\log(\nu_{\rm p}) = \begin{cases} 13.85+2.30X & \text{if } X<0 \text{ and } Y<0.3\ , \\ 13.15+6.58Y & \text{otherwise}\ , \end{cases} \tag{6}$$

where $X=0.565-1.433\alpha_{ro}+0.155\alpha_{ox}$ and $Y=1.0-0.661\alpha_{ro}-0.339\alpha_{ox}$; α_{ro} and α_{ox} are spectral slopes between 5 GHz and 5500 Å and between 5500 Å and 1 keV, respectively. The spectral slope, α_{ab}, between the a and b bands is defined as

$$\alpha_{ab} = -\frac{\log(f_a/f_b)}{\log(\nu_a/\nu_b)}\ , \tag{7}$$

where f_a is the rest-frame flux at frequency ν_a properly de-reddened for Galaxy absorption. In Table 1, we show the peak frequency, $\nu_{\rm p}$, of synchrotron radiation for each object. The average peak frequency is $\log\nu_{\rm p}=13.54\pm0.08$ for all 51 sources, $\log\nu_{\rm p}=13.90\pm0.15$ for 18 BL Lacertae objects and $\log\nu_{\rm p}=13.34\pm0.08$ for 33 FSRQs.

3 ESTIMATE OF DOPPLER FACTORS

We use the method of Zhang et al. (2002) to estimate the Doppler factor for each object in our sample. The following assumptions are made: (1) the relativistic particles satisfy a power-law distribution with a spectral index, p; (2) the radiation from radio to X-ray bands is produced by the synchrotron radiation of these particles in the jet, which gives $S(\nu)\propto\nu^{-(p-1)/2}$ for $\nu<\nu_{\rm p}$ and $S(\nu)\propto\nu^{-p/2}$ for $\nu>\nu$ (e.g. Ghisellini 1993); (3) X-ray emission is due to the synchrotron radiation above the synchrotron peak frequency; and (4) γ-rays are produced by Compton scattering of the same particles and $S(\nu)\propto\nu^{-p/2}$. Following Zhang et al. (2002), let $S_{\rm R}^{\rm obs}$, $S_{\rm O}^{\rm obs}$, $S_{\rm X}^{\rm obs}$, and $S_\gamma^{\rm obs}$ represent the observed flux densities in the radio ($\nu_{\rm R}$ in GHz), optical (V band), X-ray ($\nu_{\rm X}$ in keV) and γ-ray ($\langle E\rangle$ in units of GeV) bands respectively. Then the Doppler factors in the optical, X-ray and gamma-ray bands in the case of $\beta=3+\alpha$ can be estimated by

$$\delta_{\rm O}\approx\begin{cases} \delta_{\rm R}^{(5+p)/(6+p)}(1+z)^{-1/(6+p)}\left[a_1\frac{S_{\rm O}^{\rm obs}(\rm mJy)}{S_{\rm R}^{\rm obs}(\rm Jy)}\right]^{2/(6+p)} & \text{for } \nu_{\rm p}\le\nu_{\rm O}\ , \\ \delta_{\rm R}\left[a_2\frac{S_{\rm O}^{\rm obs}(\rm mJy)}{S_{\rm R}^{\rm obs}(\rm Jy)}\right]^{2/(5+p)} & \text{for } \nu_{\rm p}>\nu_{\rm O}\ , \end{cases} \tag{8}$$

$$\delta_{\rm X}\approx\delta_{\rm R}^{(5+p)/(6+p)}(1+z)^{-1/(6+p)}\left[10^{4.19p-9}\left(\frac{\nu_{\rm X}}{\nu_{\rm R}}\right)^{p/2}\left(\frac{\nu_{\rm p}}{\nu_{\rm R}}\right)^{-1/2}\frac{S_{\rm X}^{\rm obs}(\mu\rm Jy)}{S_{\rm R}^{\rm obs}(\rm Jy)}\right]^{2/(6+p)}\ , \tag{9}$$

and

$$\delta_\gamma\approx\delta_{\rm R}^{(5+p)/(6+p)}(1+z)^{-1/(6+p)}\left[10^{7.19p-15}\left(\frac{\langle E\rangle}{\nu_{\rm R}}\right)^{p/2}\left(\frac{\nu_{\rm p}}{\nu_{\rm R}}\right)^{-1/2}\frac{S_\gamma^{\rm obs}(\rm pJy)}{S_{\rm R}^{\rm obs}}(\rm Jy)\right]^{2/(6+p)}\ , \tag{10}$$

where $a_1 = 10^{(2.87p-6)}\nu_{\rm R}^{(1-p)/2}\ (\nu_{\rm p})^{-1/2}$ and $a_2 = 10^{(2.87p-5.87)}\ \nu_{\rm R}^{(1-p)/2}$; $\nu_{\rm p}$ is in units of 10^{15} Hz.

Table 1 A Sample of 51 Blazars

LAT Name	Source association	Class	z	$S_{\rm R}$ (Jy)	$S_{\rm O}$ (mJy)	$S_{\rm X}$ (μJy)	F_γ (ph cm^{-2} s^{-1})	α_γ	S_γ (pJy)	$\log \nu_{\rm p}$
(1)	(2)	(3)	(4)	(5)	(6)	(7)	(8)	(9)	(10)	(11)
1FGL J0050.6−0928	0048−097	BLL	0.3	1.43	1.903	0.889	4.5E–9	2.2	0.384	13.68
1FGL J0108.6+0135	0106+013	FSRQ	2.107	2.27	0.16	0.087	5.6E–9	2.54	0.815	12.74
1FGL J0112.0+2247	0109+224	BLL	0.265	1.41	1.982	3.231	5.3E–9	2.23	0.476	15.14
1FGL J0137.0+4751	0133+476	FSRQ	0.859	3.53	0.65	0.286	9.6E–9	2.34	1.029	13.44
1FGL J0217.8+7353	0212+735	FSRQ	2.367	2.67	0.849	0.051	1E–9	2.85	0.216	13.81
1FGL J0222.6+4302	0219+428	BLL	0.444	1.22	4.034	1.558	2.49E–8	1.93	1.35	14.88
1FGL J0237.9+2848	0234+285	FSRQ	1.213	2.35	0.14	0.14	3.7E–9	2.52	0.519	12.74
1FGL J0238.6+1637	0235+164	BLL	0.94	1.62	2.969	1.7	1E–9	2.02	0.063	13.83
1FGL J0334.2+3233	0333+321	FSRQ	1.263	1.6	0.364	1.6	1E–9	2.81	0.205	13.03
1FGL J0339.2−0143	0336−019	FSRQ	0.852	2.23	0.245	0.253	1.2E–9	2.5	0.164	13.15
1FGL J0423.2−0118	0420−014	FSRQ	0.915	4.37	1.002	1.087	5.6E–9	2.42	0.682	13.61
1FGL J0442.7−0019	0440−003	BLL	0.449	1.06	0.108	0.109	6.3E–9	2.44	0.79	13.01
1FGL J0501.0−0200	0458−020	FSRQ	2.291	1.07	0.11	0.07	1.1E–9	2.5	0.151	12.85
1FGL J0531.0+1331	0528+134	FSRQ	2.07	6.28	0.375	0.951	4E–9	2.64	0.67	13.05
1FGL J0608.2−0837	0605−085	FSRQ	0.872	2.01	0.546	0.325	1.9E–9	2.43	0.234	13.33
1FGL J0721.9+7120	0716+714	BLL	0.31	1.46	2.395	1.346	1.31E–8	2.15	1.027	14.75
1FGL J0738.2+1741	0735+178	BLL	0.424	0.99	1.783	0.248	4.4E–9	2.02	0.277	13.74
1FGL J0739.1+0138	0736+017	FSRQ	0.191	1.86	1.462	1.72	2.3E–9	2.63	0.379	13.56
1FGL J0757.2+0956	0754+100	BLL	0.266	1.39	3.64	0.72	2E–9	2.39	0.233	14.35
1FGL J0818.2+4222	0814+425	BLL	0.258	1.29	0.162	0.041	8.7E–9	2.15	0.682	12.88
1FGL J0830.5+2407	0827+243	FSRQ	0.94	1.67	0.33	0.22	1.3E–9	2.79	0.263	13.42
1FGL J0842.2+7054	0836+710	FSRQ	2.218	1.64	1.938	0.819	1.2E–9	2.98	0.3	14.75
1FGL J0854.8+2006	0851+202	BLL	0.306	0.6	2.639	1.063	2.7E–9	2.38	0.309	13.7
1FGL J0957.7+5523	0954+556	FSRQ	0.896	0.9	0.405	0.112	1.05E–8	2.05	0.696	13.43
1FGL J1058.4+0134	1055+018	FSRQ	0.888	3.24	0.558	0.201	7.1E–9	2.29	0.704	13.37
1FGL J1159.4+2914	1156+295	FSRQ	0.729	2.35	9.1	0.65	5.3E–9	2.37	0.596	14.33
1FGL J1221.5+2814	1219+285	BLL	0.102	0.65	3.047	0.409	6.9E–9	2.06	0.464	14.33
1FGL J1229.1+0203	1226+023	FSRQ	0.158	31.1	29.834	12.074	9.6E–9	2.75	1.833	13.6
1FGL J1256.2−0547	1253−055	FSRQ	0.536	24	2.073	1.246	3.24E–8	2.32	3.372	13.22
1FGL J1310.6+3222	1308+326	FSRQ	0.997	2.39	1.818	0.134	6.8E–9	2.3	0.683	13.98
1FGL J1421.0+5421	1418+546	BLL	0.152	0.64	1.97	0.306	9E–10	2.77	0.177	14.2
1FGL J1504.4+1029	1502+106	FSRQ	1.839	1.12	0.137	0.145	6.7E–8	2.22	5.91	12.76
1FGL J1512.8−0906	1510−089	FSRQ	0.36	1.82	1.276	0.718	4.86E–8	2.41	5.81	13.49
1FGL J1609.0+1031	1606+106	FSRQ	1.226	1.49	0.15	0.04	1.1E–9	2.72	0.203	12.94
1FGL J1613.5+3411	1611+343	FSRQ	1.397	3.41	0.553	0.194	5E–10	2.29	0.05	13.53
1FGL J1635.0+3808	1633+382	FSRQ	1.814	2.24	0.401	0.258	6.8E–9	2.47	0.889	13.44
1FGL J1642.5+3947	1641+399	FSRQ	0.593	7.44	1.135	0.914	5.6E–9	2.49	0.757	13.23
1FGL J1728.2+0431	1725+044	FSRQ	0.293	0.885	0.582	0.109	1.3E–9	2.65	0.219	13.57
1FGL J1733.0−1308	1730−130	FSRQ	0.902	7.51	0.058	0.224	3.6E–9	2.34	0.386	12.3
1FGL J1740.0+5209	1739+522	FSRQ	1.379	2.91	0.121	0.113	3.4E–9	2.71	0.623	12.8
1FGL J1751.5+0937	1749+096	BLL	0.322	4.03	1.2	0.129	6.4E–9	2.29	0.634	13.68
1FGL J1800.4+7827	1803+784	BLL	0.68	2.43	0.683	0.324	3E–9	2.35	0.327	13.4
1FGL J1807.0+6945	1807+698	BLL	0.051	1.44	5.009	0.317	1.9E–9	2.6	0.299	14.06
1FGL J1824.0+5651	1823+568	BLL	0.664	1.63	0.198	0.241	2.7E–9	2.34	0.29	13.12
1FGL J2006.0+7751	2007+777	BLL	0.342	1.08	0.819	0.158	1.4E–9	2.42	0.17	13.65
1FGL J2148.5+0654	2145+067	FSRQ	0.999	7.5	1.417	0.392	7E–10	2.56	0.105	13.59
1FGL J2202.8+4216	2200+420	BLL	0.069	3.95	5.527	0.936	7.1E–9	2.38	0.812	13.76
1FGL J2225.8−0457	2223−052	FSRQ	1.404	5.64	1.615	0.292	2.1E–9	2.53	0.302	13.72
1FGL J2232.5+1144	2230+114	FSRQ	1.037	4.94	0.701	0.486	4.1E–9	2.56	0.614	13.41
1FGL J2236.2+2828	2234+282	FSRQ	0.795	1.04	0.091	0.722	4.9E–9	2.37	0.551	12.77
1FGL J2253.9+1608	2251+158	FSRQ	0.859	7.47	1.407	1.082	4.62E–8	2.47	6.042	13.32

Table 2 Doppler Factors of 51 Blazars at Different Wavebands

LAT Name	Source association	Class	$\delta_{\rm R}$	$\delta_{\rm O}$	$\delta_{\rm X}$	δ_{γ}
(1)	(2)	(3)	(4)	(5)	(6)	(7)
1FGL J0050.6−0928	0048−097	BLL	9.6	7.94	5.78	10.89
1FGL J0108.6+0135	0106+013	FSRQ	18.4	6.54	5.01	22.64
1FGL J0112.0+2247	0109+224	BLL	9.1	7.07	4.66	6.13
1FGL J0137.0+4751	0133+476	FSRQ	20.7	8.25	5.89	20.85
1FGL J0217.8+7353	0212+735	FSRQ	8.5	3.69	1.39	4.52
1FGL J0222.6+4302	0219+428	BLL	2.6	2.65	1.39	3.7
1FGL J0237.9+2848	0234+285	FSRQ	16.1	5.29	4.93	16.64
1FGL J0238.6+1637	0235+164	BLL	24	16.84	13.1	12.08
1FGL J0334.2+3233	0333+321	FSRQ	22.2	10.56	15.86	16.85
1FGL J0339.2−0143	0336−019	FSRQ	17.4	6.73	6.33	12.24
1FGL J0423.2−0118	0420−014	FSRQ	14.59	5.58	5.33	10.45
1FGL J0442.7−0019	0440−003	BLL	12.9	5.6	5.23	22.42
1FGL J0501.0−0200	0458−020	FSRQ	15.8	5.59	4.5	12.83
1FGL J0531.0+1331	0528+134	FSRQ	31.2	8.62	10.84	20.72
1FGL J0608.2−0837	0605−085	FSRQ	7.6	3.8	2.99	6.11
1FGL J0721.9+7120	0716+714	BLL	10.8	9.49	4.87	11.24
1FGL J0738.2+1741	0735+178	BLL	3.8	3.51	1.73	4.78
1FGL J0739.1+0138	0736+017	FSRQ	8.6	6.48	6.36	8.38
1FGL J0757.2+0956	0754+100	BLL	5.6	4.45	2.46	3.93
1FGL J0818.2+4222	0814+425	BLL	4.6	2.71	1.62	10.1
1FGL J0830.5+2407	0827+243	FSRQ	13.1	5.2	4.25	9.31
1FGL J0842.2+7054	0836+710	FSRQ	16.3	11.19	4.41	6.37
1FGL J0854.8+2006	0851+202	BLL	17	18.7	12.99	20.13
1FGL J0957.7+5523	0954+556	FSRQ	6.2	3.62	2.23	10.57
1FGL J1058.4+0134	1055+018	FSRQ	12.2	4.8	3.21	11.47
1FGL J1159.4+2914	1156+295	FSRQ	28.5	20.94	8.32	18.75
1FGL J1221.5+2814	1219+285	BLL	1.2	1.68	0.82	2.24
1FGL J1229.1+0203	1226+023	FSRQ	17	12.11	8.42	9.58
1FGL J1256.2−0547	1253−055	FSRQ	24	7.4	5.85	19
1FGL J1310.6+3222	1308+326	FSRQ	15.4	8.23	3.3	13.27
1FGL J1421.0+5421	1418+546	BLL	5.1	5.15	2.63	4.58
1FGL J1504.4+1029	1502+106	FSRQ	12	4.98	4.72	38.19
1FGL J1512.8−0906	1510−089	FSRQ	16.7	9.9	7.66	34.37
1FGL J1609.0+1031	1606+106	FSRQ	25	9.3	5.65	20.07
1FGL J1613.5+3411	1611+343	FSRQ	13.7	4.7	3.12	4.8
1FGL J1635.0+3808	1633+382	FSRQ	21.5	7.89	6.37	21.32
1FGL J1642.5+3947	1641+399	FSRQ	7.8	3.43	2.98	6.25
1FGL J1728.2+0431	1725+044	FSRQ	3.8	3.03	1.64	4.4
1FGL J1733.0−1308	1730−130	FSRQ	10.7	2.35	3.38	9.42
1FGL J1740.0+5209	1739+522	FSRQ	26.5	7.65	6.97	25.45
1FGL J1751.5+0937	1749+096	BLL	12	5.33	2.42	9.62
1FGL J1800.4+7827	1803+784	BLL	12.2	6.26	4.58	10.72
1FGL J1807.0+6945	1807+698	BLL	1.1	1.43	0.55	1.16
1FGL J1824.0+5651	1823+568	BLL	6.4	3.09	3.06	7.62
1FGL J2006.0+7751	2007+777	BLL	7.9	5.66	3.1	7.23
1FGL J2148.5+0654	2145+067	FSRQ	15.6	5.55	3.41	4.87
1FGL J2202.8+4216	2200+420	BLL	7.3	5.81	3.05	6.73
1FGL J2225.8−0457	2223−052	FSRQ	16	6.63	3.55	7.92
1FGL J2232.5+1144	2230+114	FSRQ	15.6	5.39	4.46	10.51
1FGL J2236.2+2828	2234+282	FSRQ	6	2.96	5.38	11.42
1FGL J2253.9+1608	2251+158	FSRQ	33.2	11.67	9.99	39.04

In the case of $\beta = 2 + \alpha$, the corresponding Doppler factors are

$$\delta_{\rm O} \approx \begin{cases} \delta_{\rm R}^{(3+p)/(4+p)}(1+z)^{-1/(4+p)}\left[b_1\frac{S_{\rm O}^{\rm obs}({\rm mJy})}{S_{\rm R}^{\rm obs}({\rm Jy})}\right]^{2/(4+p)} & \text{for } \nu_{\rm p} \le \nu_{\rm O}\ , \\ \delta_{\rm R}\left[b_2\frac{S_{\rm O}^{\rm obs}({\rm mJy})}{S_{\rm R}^{\rm obs}({\rm Jy})}\right]^{2/(3+p)} & \text{for } \nu_{\rm p} > \nu_{\rm O}\ , \end{cases} \tag{11}$$

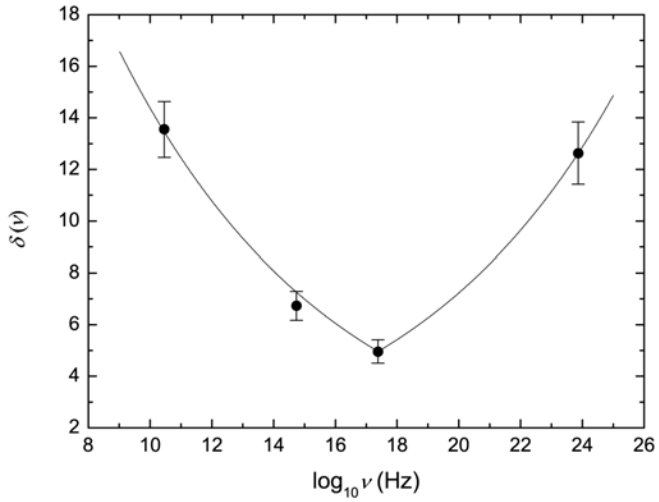

Fig. 1 Variation of the Doppler factor with frequency in the case of the continuous jet. The filled circles with error bars represent the average Doppler factors in the radio, optical, X-ray and γ-ray bands and the solid curve is given by Eq. (14).

$$\delta_{\rm X} \approx \delta_{\rm R}^{(3+p)/(4+p)}(1+z)^{-1/(4+p)}\left[10^{4.19p-9}\left(\frac{\nu_{\rm X}}{\nu_{\rm R}}\right)^{p/2}\left(\frac{\nu_{\rm p}}{\nu_{\rm R}}\right)^{-1/2}\frac{S_{\rm X}^{\rm obs}(\mu{\rm Jy})}{S_{\rm R}^{\rm obs}({\rm Jy})}\right]^{2/(4+p)}, \quad (12)$$

and

$$\delta_{\gamma} \approx \delta_{\rm R}^{(3+p)/(4+p)}(1+z)^{-1/(4+p)}\left[10^{7.19p-15}\left(\frac{\langle E\rangle}{\nu_{\rm R}}\right)^{p/2}\left(\frac{\nu_{\rm p}}{\nu_{\rm R}}\right)^{-1/2}\frac{S_{\gamma}^{\rm obs}({\rm pJy})}{S_{\rm R}^{\rm obs}({\rm Jy})}\right]^{2/(4+p)}, \quad (13)$$

respectively, where $b_1 = 10^{(2.87p-6)}\nu_{\rm R}^{(1-p)/2}\ (\nu_{\rm p})^{-1/2}$ and $b_2 = 10^{(2.87p-5.87)}\ \nu_{\rm R}^{(1-p)/2}$.

Using the above formula and known radio Doppler factors given in Table 1, we can estimate the Doppler factors in the optical, X-ray and γ-ray bands for each object. In order to do so, we assume that the spectral index of the relativistic particles is $p = 2.2$, thus our results in this case of $p = 2.2$ and $\beta = 2 + \alpha$ (corresponding to the case of the continuous jet) are shown in Table 2. It can be seen from Table 2 that the Doppler factors in different bands are different. Moreover, the averaged values of the Doppler factors at different bands for the sample are $\langle\delta_{\rm O}\rangle = 7.73 \pm 0.56, \langle\delta_{\rm X}\rangle = 4.96 \pm 0.45$, and $\langle\delta_{\gamma}\rangle = 12.63 \pm 1.21$, respectively, where the averaged γ-ray energy of 51 blazars is $\langle E\rangle = 3.02 \pm 0.10$ GeV. This result is shown in Figure 1. It is clear that there is a concave shape of the averaged Doppler factor changing with frequency, i.e. the Doppler factor decreases with frequency from radio to X-ray bands and increases from X-ray to γ-ray bands and the averaged Doppler factors at radio and γ-ray bands are almost same. Such a concave shape is consistent with that given by Zhang et al. (2002), but the values of the averaged Doppler factors here are larger than those given by Zhang et al. (2002). From Table 2, several sources do not follow such a pattern, for example the Doppler factor for J0238+1637 decreases from radio to γ-ray bands, and the optical Doppler factors for J0334.2+3233 and J0531.0+1331 are lower than the X-ray Doppler factors.

Obviously, the Doppler factors at different bands in the case of $\beta = 3 + \alpha$ are different from those in the case of $\beta = 2 + \alpha$. We also calculate the Doppler factors for each object in the case of $\beta = 3 + \alpha$, so the averaged values of the Doppler factors at different bands for the sample are: $\langle\delta_{\rm O}\rangle = 7.88 \pm 0.61, \langle\delta_{\rm X}\rangle = 6.25 \pm 0.51$, and $\langle\delta_{\gamma}\rangle = 12.61 \pm 1.09$, also indicating a concave shape.

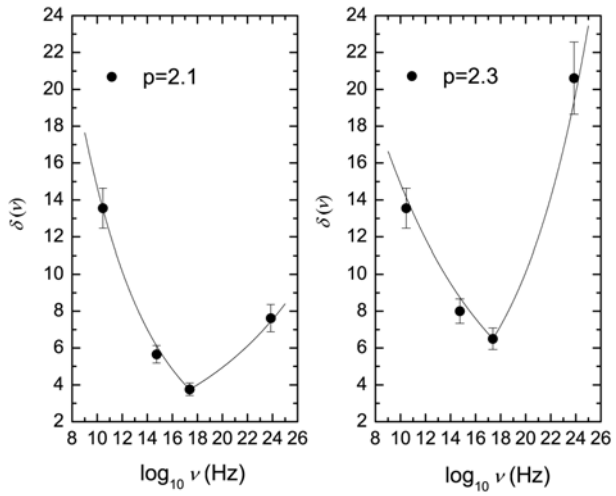

Fig. 2 Variation of the Doppler factor with frequency ($p = 2.1$ and 2.3). The filled circles with error bars represent the average Doppler factors in the radio, optical, X-ray and γ-ray bands .

Since the spectral index p of the relativistic particles is an important parameter in our estimate of Doppler factors at optical, X-ray and gamma-ray bands, we also calculate the Doppler factors at these bands for different values of $p = 2.1$ and $p = 2.3$. The averaged Doppler factors of the sample in the case of $\beta = 2 + \alpha$ with $p = 2.1$ and 2.3 are shown in Figure 2. It can be seen that Doppler factors at optical, X-ray and gamma-ray bands strongly depend on the values of parameters p. Although there is a concave shape, a significant difference between the averaged gamma-ray Doppler factors for a lower value (2.1) and a higher value (2.3) of p appears. From Figures 1 and 2, the averaged gamma-ray Doppler factor increases with p.

Finally, we try to give an empirical expression from our analysis. We find that the averaged Doppler factors satisfy the following relation:

$$\delta_\nu = \begin{cases} \delta_{\rm X}^{1+0.09\log(\nu_{\rm X}/\nu)}, & \text{if } \nu < \nu_{\rm X}, \\ \delta_{\rm X}^{1-0.09\log(\nu_{\rm X}/\nu)}, & \text{if } \nu > \nu_{\rm X}. \end{cases} \tag{14}$$

For the case of $\beta = 2 + \alpha$ and $p = 2.2$, and

$$\delta_\nu = \begin{cases} \delta_{\rm X}^{1+0.06\log(\nu_{\rm X}/\nu)}, & \text{if } \nu < \nu_{\rm X}, \\ \delta_{\rm X}^{1-0.06\log(\nu_{\rm X}/\nu)}, & \text{if } \nu > \nu_{\rm X}. \end{cases} \tag{15}$$

for the case of $\beta = 3 + \alpha$ and $p = 2.2$. The results are consistent with those given by Zhang et al. (2002), but the parameters are different. Our result suggests that the emissions from a blazar at different wavebands are produced in different emission regions or in the same emission region with a different viewing angle. It should be noted that Fan et al. (1993) found that the Doppler factors in radio, optical, and X-ray bands satisfy $\delta_{\rm R} > \delta_{\rm O} > \delta_{\rm X}$ and can be expressed in the form $\delta(\nu) \sim \delta_{\rm O}^{1+1/8\,\log(\nu_{\rm O}/\nu)}$. Cheng et al. (1999) showed that the relation for the Doppler factor with frequency can be expressed in the form of $\delta(\nu) \sim \delta_{\rm X}^{1-0.28\,\log(\nu_{\rm X}/\nu)}$ for the X-ray to γ-ray spectra of 3C 279.

4 CORRELATION BETWEEN THE DOPPLER FACTOR AND THE PEAK FREQUENCY

BL Lacertae objects and FSRQs are two subgroups of active galactic nuclei. Although they show many common properties, there are some differences from an observational point of view. In the present work, the average peak frequency of BL Lacertae objects, log$\nu_{\rm p} = 13.90$, is higher than that of FSRQs, log $\nu_{\rm p} = 13.34$.

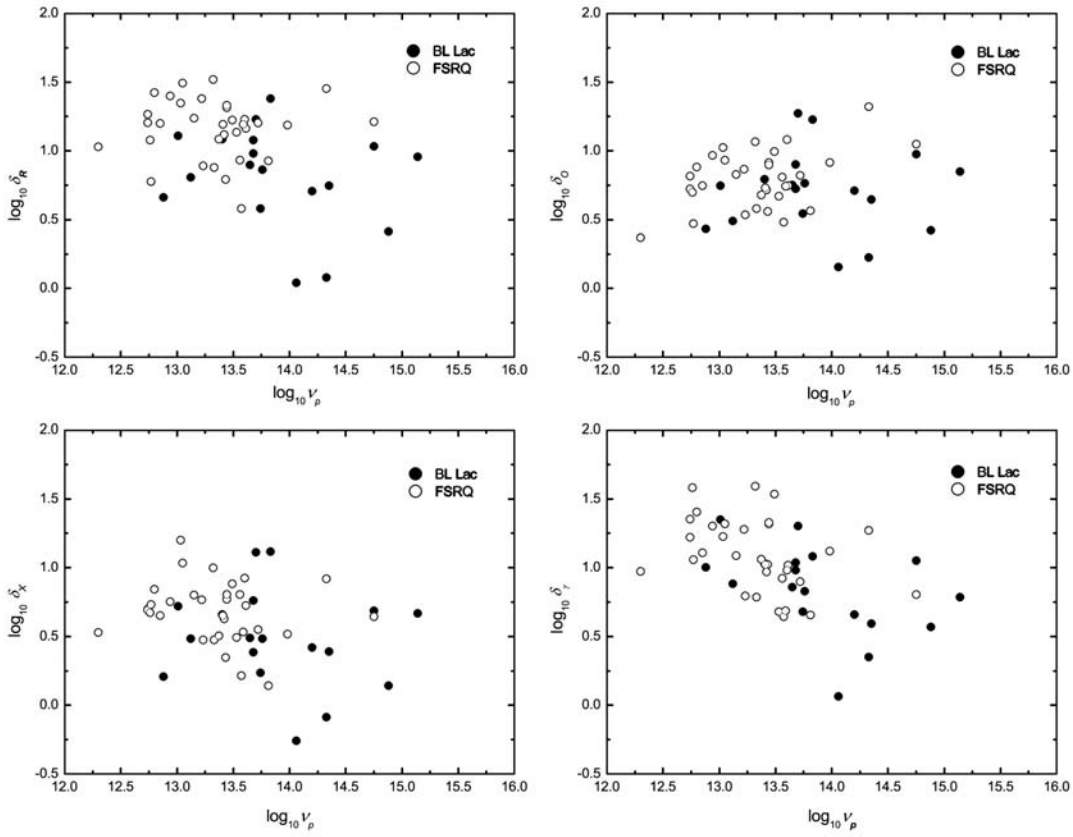

Fig. 3 Relation between the synchrotron peak frequency and the Doppler factor. The filled points are for BL Lacertae objects and the open circles are for FSRQs.

In Figure 3, we show the relations between the Doppler factors at radio, optical, X-ray, and gamma-ray bands and the peak frequency of synchrotron radiation. We find the following relations: $\log \delta_{\rm R} = -0.181 \log \nu_{\rm p} + 3.488$ with $r = 0.335$ and $P = 1.61 \times 10^{-2}$, $\log \delta_{\rm X} = -0.134 \log \nu_{\rm p} + 2.426$ with $r = 0.274$ and $P = 0.051$, and $\log \delta_{\gamma} = -0.264 \log \nu_{\rm p} + 4.576$ with $r = 0.511$ and $P = 1.279 \times 10^{-4}$. Obviously, there are marginal anti-correlations between $\delta_{\rm R}$ and $\nu_{\rm p}$ and between $\delta_{\rm X}$ and $\nu_{\rm p}$, but there is a strong anti-correlation between δ_{γ} and $\nu_{\rm p}$. Regarding the Doppler factors in the optical band, there is no correlation between $\delta_{\rm O}$ and $\nu_{\rm p}$.

We also give plots of the Doppler factors and the flux densities at different bands in Figure 4 and find the following correlations: $\log \delta_{\rm R} = 0.414 \log S_{\rm R} + 0.898$ with $r = 0.468$ and $P = 5.372 \times 10^{-4}$, $\log \delta_{\rm X} = 0.225 \log S_{\rm X} + 0.704$ with $r = 0.393$ and $P = 4.32 \times 10^{-3}$, and $\log \delta_{\gamma} =$

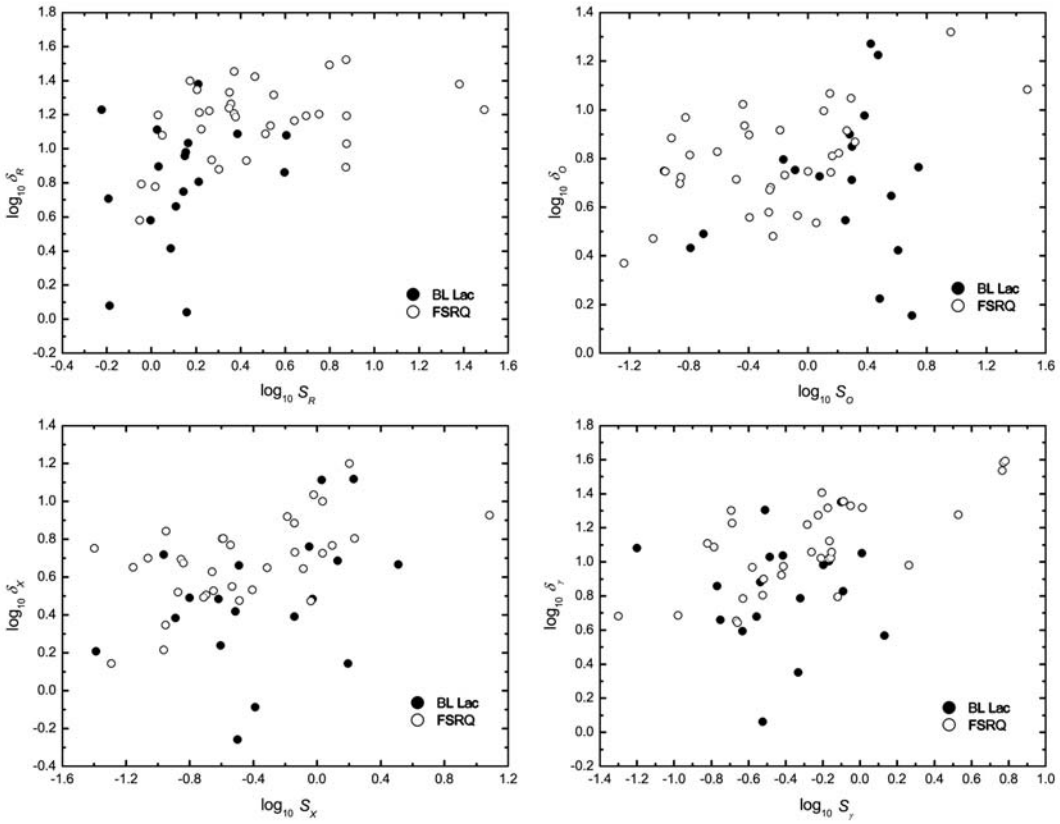

Fig. 4 Relation between the flux density and the Doppler factor. The filled points are for BL Lacertae objects and the open circles are for FSRQs.

$0.359 \log S_\gamma + 1.118$ with $r = 0.512$ and $P = 1.224 \times 10^{-4}$. Again, there is no correlation in the optical band. There are marginal correlations between $\delta_{\rm R}$ and $\nu_{\rm p}$ and between $\delta_{\rm X}$ and $\nu_{\rm p}$, but there is a strong correlation between δ_γ and $\nu_{\rm p}$.

5 CONCLUSIONS

In this paper, we study the possible variation of Doppler factor with frequency by using an enlarged sample and the methods of Zhang et al. (2002). We have confirmed the result for multiwavelength Doppler factors given by Zhang et al. (2002), i.e. the Doppler factor decreases with frequency from radio to X-ray bands and increases from X-ray to γ-ray bands, indicating a concave shape. Moreover, the spectral index p of relativistic particles has an important role in the estimate of the Doppler factors at optical, X-ray, and gamma-ray bands and these Doppler factors increase with increasing p. On the other hand, we have given the correlations between the multiwavelength Doppler factors and the peak frequency of synchrotron radiation as well as between the Doppler factors and the flux densities at radio, optical, X-ray and gamma-ray bands. Our results have shown that there are strong correlations between δ_γ and $\nu_{\rm p}$ as well as between δ_γ and S_γ.

It should be pointed out that further observed data, especially in the radio band, are needed in order to further study the multiwavelength Doppler factors for gamma-ray loud blazars.

References

Abdo A.A., Ackermann M., Ajello M., et al. 2010, ApJ, 715, 429
Blandford, R. D., & Konigl, A. 1979, ApJ, 232, 34
Bloom, S. D., & Marscher, A. P. 1996, ApJ, 461, 657
Cheng, K. S., Zhang, L., & Fan, J.-H. 1999, Acta. Astrophys. Sin., 19, 251
Cheng, K. S., Zhang, X., & Zhang, L. 2000, ApJ, 537, 80
Ciliegi, P., Bassani, L., & Caroli, E. 1995, ApJ, 439, 80
Dermer, C. D., Schlickeiser, R., & Mastichiadis, A. 1992, A&A, 256, L27
Dermer, C. D., Sturner, S. J., & Schlickeiser, R. 1997, ApJS, 109, 103
Fan, J. H., Xie, G. Z., Li, J. J., Liu, J., Wen, S. L., Huang, R. R., Tang, Z. M., & Wang, Y. J. 1993, ApJ, 415, 113
Fossati, G., Maraschi, L., Celotti, A., Comastri, A., & Ghisellini, G. 1998, MNRAS, 299, 433
Ghisellini, G. 1993, Adv. Space Res., 13, 587
Ghisellini, G., Celotti, A., Fossati, G., Maraschi, L., & Comastri, A. 1998, MNRAS, 301, 451
Ghisellini, G., & Maraschi, L. 1989, ApJ, 340, 181
Hovatta, T., Valtaoja, E., Tornikoski1, M. & Lähteenmäki1, A. 2009, A&A, 494, 527
Lind, K. R., & Blandford, R. D. 1985, ApJ, 295, 358
Maraschi, L., Ghisellini, G., & Celotti, A. 1992, ApJ, 397, L5
Padovani, P., & Giommi, P. 1995, ApJ, 444, 567
Padovani, P., Perlman, E. S., Landt, H., Giommi, P., & Perri, M. 2003, ApJ, 588, 128
Savolainen, T., Homan, D. C., Hovatta, T., Kadler, M., Kovalev, Y. Y., Lister, M. L., Ros, E., & Zensus, J. A. 2010, A&A, 512, A24
Sikora, M., Begelman, M. C., & Rees, M. J. 1994, ApJ, 421, 153
Teräsranta et al., 2004, A&A 427, 769
Zhang, L., & Cheng, K. S. 1997, ApJ, 488, 94
Zhang, L., Fan, J.-H., & Cheng, K.-S. 2002, PASJ, 54, 159